Applied Intelligence (2021) 51:4664–4681
https://doi.org/10.1007/s10489-020-02104-5

Bio-inspired self-organized cooperative control consensus for crowded UUV swarm based on adaptive dynamic interaction topology

Hongtao Liang [1] · Yanfang Fu [2] · Jie Gao [1]

Accepted: 27 November 2020 / Published online: 5 January 2021

Abstract
Cooperative control is currently a challenging topic of crowded unmanned underwater vehicle (UUV) swarm. However, individual behavior conflict and chain-avalanche collision involved in this swarm are easily triggered due to the fluctuations and disturbances. In order to address the two problems, a bio-inspired self-organized cooperative control consensus derived from adaptive dynamic interaction topology is investigated in this paper. Firstly, a novel following-interaction framework incorporating the topological interaction and visual interaction is devised to ensure the minimum number and optimal distribution for neighborhoods. Then, an adaptive dynamic computing model inspired by single-nearest-neighbor following and weighted- multiple-nearest-neighbors following is proposed to steer a sensitive following behavior, in which the influence of each individual on this following behavior is described by a nonlinear weight. Finally, a distributed control protocol is put forward by using the proposed following model and mathematics-based potential fields to achieve the cohesive flocking and avoiding collision, and its sufficient conditions is proven by Laypunov and LaSalle invariance principle to accomplish a self- organized cooperative control. Simulation results are presented for illustrating the feasibility and effectiveness of our proposed control approach.

Keywords Unmanned underwater vehicle · Bio-inspired computing · Self-organizing · Cooperative control · Following-interaction

1 Introduction

Unmanned underwater vehicle (UUV) is an imperative vehicle in oceanic engineering over the past decades, which has a wide application for monitoring, exploration and surveillance, especially in hazardous environment [1–5]. However, due to the limited robustness and adaptability of existing rigid-formation control methods for more complex missions [3], a crowded UUV swarm composed of a large number of homogeneous/heterogeneous and low-cost submersible intelligent robots, has been aroused more compelling interest. However, the cooperative control for this swarm is a challenge because individual behavior conflict and chain avalanche collision derived from unknown fluctuations and disturbances are easily triggered [5].

How to overcome the conflict and collision involved in the crowded UUV swarm, increasing attentions have been paid to self-organized cooperative control [6, 7]. The essence of this control approach in swarm represents a coordination of a group agents to generate and maintain a pattern in a self-organized way. Up to now, numerous studies on self-organized cooperative control have been developed, all of which can be divided into centralized and distributed control manners [7–28]. The centralized manner generally adopts a top-down modeling, where an upper controller is employed to perform the global mission. However, this scheme is vulnerable and unavailable in real applications [8]. Conversely, the distributed manner formed by down-top modeling is attracted more attentions, when a large number of agents are involved. More recently, various approaches in distributed manner have been proposed, such as leader-following [9], virtual structure [10, 11], artificial potential field [12, 13], and consensus control [14, 15].

Leader-following, as a distinguished pattern, is essentially a predefined distributed pattern to achieve a swarm control due to

✉ Hongtao Liang
lianghongtao.789@163.com

[1] School of Physics and Information Technology, Shaanxi Normal University, Xian 710119, China

[2] School of Computer Science and Engineering, Xi'an Technological University, Xi'an 710032, China

its simplicity and reliability, in which all following agents track a real or desired leader to maintain a specific orientation and distance among agents. For example, Wang et al. [9] proposed a leader-following formation based on sliding mode control for autonomous underwater vehicles (AUVs). Despite existing significant theoretical formalization, this scheme has a fatal limitation that the formation pattern is rigid.

In order to tackle the above weakness of leader-following scheme, the virtual structure approach is developed, where the swarm is regarded as a tight or loose entity and its desired position is assigned to a structure. Basant et al. [10] presented a formulation of cooperative control for a group of AUVs, in which a virtual flocking center was predicted by consensus protocol. Yang et al. [11] proposed a novel formation control based on Jacobi shape for multi-AUVs, where the geometric shape was designed to track a desired trajectory. However, a structure generated in this method is unavailable for avoiding collision, which may take more sensing and computing costs due to the adverse robustness.

To overcome the drawback of strict geometric relationship in both leader-following and virtual structure, the artificial potential field is provided, where each agent moves according to a gradient direction of potential field generated by total sum of all virtual attractive and repulsive forces. Pan et al. [12] designed a distributed formation control based artificial potential field to accomplish an AUV formation. In addition, Zhu et al. [13] designed a self-organized artificial potential filed formation control to avoid obstacles and replan paths for UUV formation. Although the aforementioned works are effective, there exist two common limitations, i.e., local minimum and deadlock phenomenon, when one obtains multiple attractive and repulsive forces, so adaptability is relatively weak.

Consensus control method has been widely utilized in cooperative control fields, where agents make use of information exchange to reach a common consensus on velocity or orientation for a cohesive swarm. Hu et al. [14] stated a consensus for multi-agents with antagonistic interactions and communication noises. Cai et al. [15] investigated a leader-following output consensus for discrete-time multi-agent systems with uncertainties. Apparently, these consensus-based methods are all based on an ideal communication, and the influence of each individual on formation pattern is ignored or simplified.

Unfortunately, some above-mentioned techniques on distributed control are only available for desired environment and lack the self-organized cooperative behavior. In fact, the UUV is always exposed to the disturbed environment, and its sensing and communicating are limited. Therefore, developing high-performance cooperative control is a major challenging task in real application. Behavior-driven methods [7, 16–28] inspired by collective behaviors in nature, such as a school of fish, a flock of birds, a herd of sheep and a swarm of ants, have received considerable attentions in the field of cooperative control. Two existing modeling styles, swarm-based macroscopic mode and individual-based microscopic mode, are employed to design a behavior-driven method. The former study works on an entire larger-scale swarm while ignoring all underlying interactions. Conversely, the latter focuses on how to describe the cluster motion via individual interaction. Due to intuitive and appealing interaction potentials, the latter has gained increasing interest in cooperative control.

As one landmark work, Reynolds et al. [17] primarily introduced a distinguished swarm model, so-called Boids, in which three behavioral rules, attraction, repulsion and alignment, were devised to establish a flock. Based on this, various models such as Vicsek [18], Couzin [20], and social force model [21], have been proposed for swarm coordination. The importance of aforementioned works is that it successfully shows the behavioral emergence of a group only influenced by its neighbors and environment [19]. However, most previous works devote on the velocity-average mechanism to achieve rendezvous, cohesion and consensus, in which more heterogeneous characteristics are ignored in local interaction.

In recent past decade, with a rapidly technical development of target tracking, image processing, and data analysis, more hidden interactions are excavated such as topological interaction [22], single-neighbor following [23], multiple-nearest-neighbors following [24], visual perception and attention [25]. The above interactions not only reveal the inherent mechanism of behavioral emergence, but also provide some solutions for self-organizing cooperative control. Duan et al. [26] designed a hierarchical network with behavior learning mechanism inspired by single-neighbor following in pigeon flocking, thereby achieving an unmanned aerial vehicle formation control. Liang et al. [27] presented a behavior-driven cooperative control strategy, in which multiple neighbors can form an immune network to achieve an intelligent swarm of UUVs. Yang et al. [28] proposed a control strategy for time-delay self-organized fission behavior of flocking system. Although most above-mentioned works can achieve a cooperative control, the lower synchronous velocity still exists and the robustness against disturbances is terrible, especially under the unpredictable ocean, which may easily trigger conflicts and collisions.

Motivated by above observations, this paper considers the cooperative control problem for crowded UUV swarm. A novel bio-inspired self-organized cooperative control approach inspired by intelligent perception and interactive computing from various biological clusters is creatively proposed. Firstly, a following interaction framework is designed to ensure the minimum number and optimal distribution of the neighborhood via the topological interaction and visual interaction. Then, a novel computing model involved with single-nearest-neighbor following (SNNF) and weighted multiple-nearest-neighbors following (WMNNF) is proposed to achieve an adaptive and dynamic following process, and the influence of individual on the sensitive behavior is described by a nonlinear weight, which is essentially a non-average

velocity mechanism unlike the traditional average-mechanism. Moreover, a cooperative control protocol based on the proposed following model and potential field, is designed to achieve a self-organized flocking for crowded UUV swarm. Simulation results demonstrate that our approach can accomplish the cooperative control with a higher effectiveness and robustness in comparison to the existing methods. The main contributions of this paper are summarized as follows:

(i) A bio-inspired self-organized cooperative control consensus derived from adaptive dynamic interaction topology is firstly proposed for the crowded UUV swarm, by elaborately configuring the latest intelligent perceptions and interactive computing mechanisms.
(ii) An adaptive dynamic interaction topology is creatively proposed to steer interactions via the minimum number and optimal distribution of neighborhoods, which is essentially a non- average mechanism considering unlike the previous average-mechanism [17–21].
(iii) A self-organized cooperative control protocol is designed by using the proposed following model and mathematics-based potential fields, which can effectively achieve the swarm cohesion and avoiding collision to solve the individual behavior conflict and chain-avalanche collision.
(iv) In formulating the proposed approach, three quantitative indexes, such as mean heading, orderness parameter, and scale parameter, are devised to prove that the robustness and efficiency of our approach are better than that of the existing approaches.

The remaining of this paper is organized as follows. Section 2 describes preliminary knowledge and problem statement. Section 3 presents an adaptive dynamic interaction topology. Section 4 designs a self-organized cooperative control protocol. Section 5 performs all simulations. Finally, a conclusion is given in Section 6.

2 Preliminary knowledge and problem statement

2.1 Local interaction

It has been revealed that the local interaction can describe the collective behavior of biological cluster in [19–28]. In the formulating the local interaction, how to describe an individual action influenced by effects from its neighbors is a key topic. Up to now, the topological interaction, visual interaction, single-nearest-neighbor synergy and multiple-nearest-neighbors synergy have been investigated by bio-inspired scientists in physics and engineering [22–25].

For topological interaction, it was firstly discovered in analyzing the flight data of starlings [29], where each individual in the group only interacts with the nearest 6 or 8 neighbors. This study subverts a traditional definition of neighbor that an individual can interact with all neighbors who is within a fixed distance as shown in Fig. 1a. The reason for this difference is that a specific number of neighbors is subject to the cortical elaboration of prenumeric ability, rather than individual's perception ability. It is reported that an interaction network formed by topological interaction, as shown in Fig. 1b, has a trade-off between perceived cost and group robustness [30].

For visual interaction, it is implied that the visual perception and visual attention can provide a solution to depict individual interactions in biological cluster. (i) The visual

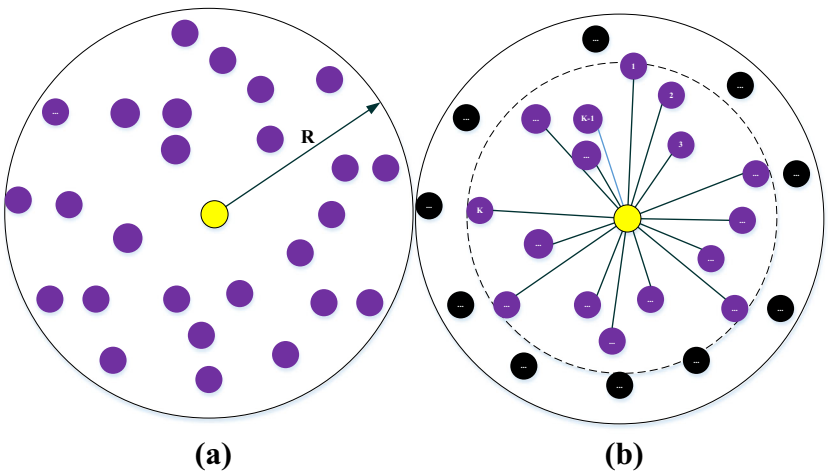

Fig.1 **a** Distance Interaction and **b**Topological Interaction. **a** The distance interaction selects all neighbors in a specific fixed distance, i.e., sensing region marked by solid circle with radius *R*. Most of the existing models, i.e., Boids [17], Vicsek [18], and Couzin [20], all rely on this aprioristic assumption. **b** The topological interaction can generate the interactions within a fixed number of neighbors, for example the specific *k* in a dotted circle, whose radius is less than that of distance interaction. Compared with the distance interaction, this interaction is more suitable to keep cohesion in the presence of fluctuations and disturbances

perception can sense all neighbors around within the sensing range, which is based on limited view (blindness angles). It is intuitively expected to improve synchronization motion as shown in Fig. 2a. (ii) The visual attention is an important psychological mechanism to select the most relevant information from limited view [25], i.e., it can discard a large amount of background information to achieve an efficient screening, as illustrated in Fig. 2b. Hence, some metaphorical mechanisms inspired by visual interaction can be useful to guide the cohesion and avoidance [31].

For single-nearest-neighbor synergy, it states that the individual only tracks a single neighbor. For example, a school of fishes is dominated by an intermittent pairwise interaction between the individual and its nearest neighbor [21]. Similarly. Herbert et al. [32] used a neural network to analyze the tracking behavior in shoaling fish, revealed that each individual actually responded only to the nearest neighbor. In addition, a single-nearest-neighbor synergy based on hierarchical relationship was ensconced in pigeon-Inspired optimization [33]. Clearly, a distinct advantage of this mechanism is smaller computing cost, which is conducive to improving the robustness and sensitiveness.

For multiple-nearest-neighbors synergy, its essence is that an individual can synthesize all influences from multiple-nearest neighbors to make decision for its behavior. Due to its robustness for collective behaviors, several popular models, such as Boids, Vicsek and Couzin [19], all adopt this synergy. However, existing works are all based on velocity-average mechanism, in which accompanying properties, i.e., sensing, communicating, influencing and decision-making abilities, are ignored in this procedure. Actually, these features play an important role in achieving a collective behavior. It was reported that influences from multiple-nearest neighbors have nonlinear characteristic, rather than a simple linear superposition [34]. Thus, the non-average mechanism involved in multiple-nearest-neighbors synergy is a worthy of discussing in flocking control.

2.2 Graphs theory

It is convenient to model the neighbor interactions between agents by an undirected or directed graph [35], where an individual UUV is regarded as a node and the interconnection topology in UUV swarm can be described as a graph.

Suppose that a graph $G(V, E, A)$ consists of a node set $V = \{v_1, v_2, \cdots, v_n\}$ and a edge set$E \subseteq V \times V$, in which each edge is a pair of vertices (v_i, v_j) such as $i \neq j$. If $(v_i, v_j) \in E$, then one usually says that i and j are adjacent.$A = [a_{ij}] \in \mathbb{R}^{n \times n}$ is defined as adjacent matrix which is an integer matrix with rows and columns indexed by vertices, such that $(v_i, v_j) \in E$ is equal to $a_{ij} = 1$, else $a_{ij} = 0$. The Laplacian matrix $L = [l_{ij}] \in \mathbb{R}^{n \times n}$ is denoted by $L = D\text{-}A$, where $D = [d_{ij}]$ is a diagonal matrix with $d_{ij} = \sum_{j=1}^{n} a_{ij}$. The neighbor set for agent i is denoted as $N_i = \{v_j \in V | (v_i, v_j) \in E\}$.

Remark 1: *If* $(v_i, v_j) \in E \Leftrightarrow (v_j, v_i) \in E$, *G is an undirected graph, else it is called a directed graph. Furthermore, G is strongly connected if there is a directed path from* (v_i, v_j) *and* (v_j, v_i)*between any pair of distinct nodes* v_i *and* v_j. *A spanning tree of a directed graph is a directed tree formed by graph edges that connect all nodes of the graph.*

Lemma 1: *For a connected graph G, its L is symmetrical and positive semidefinite, and all eigenvalues are non-negative real number which denoted by* $\lambda_i \in \mathbb{C}$ *with an ascending order in magnitude,* i.e.,$0 = \lambda_1(L) \leq \lambda_2(L) \leq \cdots \leq \lambda_n(L)$.

2.3 Problem statement

Consider a group of N agents in the crowded UUV swarm, labeled 1,..., N, moving in horizontal plane. For agent i, its kinematic and dynamic with six-Degree of Freedom can be given by

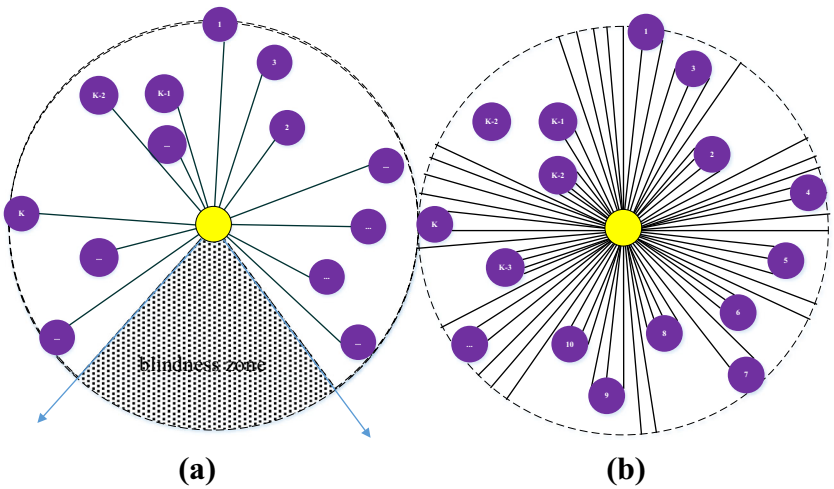

Fig.2 **a** Visual Perception and **b** Visual Attention

$$\begin{cases} \dot{\eta}_i = J(\psi_i)v_i \\ M_i\dot{v}_i + C_i(v_i)v_i + D_i(v_i)v_i + g_i(\eta_i) = \tau_i + w_i \end{cases} \tag{1}$$

where $\eta_i = [x_i, y_i, \psi_i]^T \in \mathbb{R}^3$ is the positions and yaw angle in earth-fixed frame, respectively. $v_i = [u_i, v_i, r_i]^T \in \mathbb{R}^3$ is the velocity vector in body-fixed frame, where u_i is a surge velocity, v_i is a sway velocity, and r_i is an angular yaw velocity. $\tau_i = [\tau_{iu}, 0, \tau_{ir}]^T \in \mathbb{R}^3$ is a control input vector, and $g_i = [g_{iu}, g_{iv}, g_{ir}]^T \in \mathbb{R}^3$ denotes the generalized gravitational and buoyancy forces, and $w_i = [w_{iu}, w_{iv}, w_{ir}]^T \in \mathbb{R}^3$ denotes total unknown external disturbances caused by winds, waves and ocean currents. M_i, $C_i(v_i)$ and $D_i(v_i)$ are the inertia matrix, Coriolis matrix and damping matrix, respectively. The $J_i(\psi_i)$ is a transformation matrix given by

$$J_i(\psi_i) = \begin{bmatrix} \cos\psi_i & -\sin\psi_i & 0 \\ \sin\psi_i & \cos\psi_i & 0 \\ 0 & 0 & 1 \end{bmatrix} \tag{2}$$

Due to the hydrodynamic performance induced by the assumption of symmetry in plane and vertical directions, $g_i = [g_{iu}, g_{iv}, g_{ir}]^T = 0$. Moreover, the technique of state feedback linearization is utilized to simplify the kinematic and dynamic model into a general double-integrator model [36].

Specifically, the nonlinear model (1) can be written as

$$\begin{bmatrix} \dot{\boldsymbol{\eta}}_i \\ \dot{\boldsymbol{v}}_i \end{bmatrix} = \begin{bmatrix} I & 0 \\ 0 & -\boldsymbol{M}_i^{-1} \end{bmatrix} \begin{bmatrix} \boldsymbol{J}(\psi_i)\boldsymbol{v}_i \\ \boldsymbol{N}(\boldsymbol{v}_i)\boldsymbol{v}_i \end{bmatrix} + \begin{bmatrix} 0 \\ \boldsymbol{M}_i^{-1}\boldsymbol{G}(\zeta) \end{bmatrix} \widehat{u}_i \tag{3}$$

where $N(v_i)v_i = C_i(v_i)v_i + D_i(v_i)v_i, G(\zeta)$ denotes the hydrodynamic coefficients, and $\widehat{u}_i = [T_u, T_v, T_r]$ denotes the sum of forces and rudder angles.

Defining $\xi_i = [\eta^{\mathrm{T}}, v^{\mathrm{T}}]^{\mathrm{T}}$ and $h(\xi_i) = \eta$, a standard nonlinearization function can be obtained from (3) as follows

$$\begin{cases} \dot{\xi}_i = f(\xi_i) + g(\xi_i)\widehat{u}_i \\ \zeta_i = h(\xi_i) \end{cases} \tag{4}$$

where

$$f(\xi_i) = \begin{bmatrix} I & 0 \\ 0 & -\boldsymbol{M}_i^{-1} \end{bmatrix} \begin{bmatrix} \boldsymbol{J}(\psi_i)\boldsymbol{v}_i \\ \boldsymbol{N}(\boldsymbol{v}_i)\boldsymbol{v}_i \end{bmatrix}, g(\xi_i) = \begin{bmatrix} 0 \\ \boldsymbol{M}_i^{-1}\boldsymbol{G}(\zeta) \end{bmatrix}, \widehat{u}_i \text{ is}$$

the input of this nonlinear system.

Then, a new transformed coordination with $p_i = [h_i(\xi)]^{\mathrm{T}} \in \mathbb{R}^3$ and $q_i = [\partial_f\ h_i\ (\xi)]^{\mathrm{T}} \in \mathbb{R}^3$ is defined by derivative of $h(\xi_i)$, and its corresponding control input can be defined as

$$u_i = B(\xi_i) + \Gamma(\xi_i)\widehat{u}_i \tag{5}$$

where $B(\xi_i) = \left[\partial_f^2 h_i(\xi)\right]^{\mathrm{T}}$, and $\Gamma(\xi_i) = [\partial_g \partial_f h_i(\xi_i)] \in \mathbb{R}^{3\times 3}$.

Thus, the motion model (1) can be represented by a second-order integrator model by (3) and (4), as follows

$$\begin{cases} \dot{p}_i = q_i \\ \dot{q}_i = u_i \end{cases} \quad (i = 1, 2..., N) \tag{6}$$

where $p_i \in \mathbb{R}^3$ and $q_i \in \mathbb{R}^3$ are the position and velocity variables of agent i, respectively, and u_i is the control input.

In addition, an underlying interaction topology among agents may dynamically change, which can be described by neighbor set in a connected graph, as follows

$$N_i(t) = \left\{ j | d_{ij}(t) \le R_i, j \in \{1, \cdots, N\}, j \ne i \right\} \tag{7}$$

where R_i is the sensing radius of agent i, and $d_{ij}(t) = \|p_i - p_j\|$ is an Euclidean distance between agent i and agent j.

Remark 2: *The neighbor graph is essentially a distance-dependent and time-varying topology, there are two reasons given by (i) each agent has a nonuniform sensing strength due to the factors such as limited perception range and narrow motion-space in scale effects, and (ii) all agents are influenced by external disturbances composed of information loss, delayed communication and noises.*

Assumption 1: *The velocity is bounded to prevent the collisions caused by motion inertia, which is given by*

$$q_i = \begin{cases} q_i, & \|q_i\| \le V_{\max} \\ V_{\max}\dfrac{q_i}{\|q_i\|}, & \|q_i\| > V_{\max} \end{cases} \tag{8}$$

where $V_{\max}$ is the maximum velocity.

In this paper, our objective is to design a self-organized cooperative control that can guarantee that the crowded UUV swarm can achieve the cohesive flocking and collision avoiding without any splits, under the assumption that the initial network is a connected graph. In particular, the objectives of this paper are formulated as

$$\lim_{t\to\infty} \|p_i(t) - p_j(t)\| \le R, \quad (i, j \in N) \tag{9}$$

$$\lim_{t\to\infty} \|p_i(t) - p_j(t)\| \ge D, \quad (i, j \in N) \tag{10}$$

$$\lim_{t\to\infty} \|q_i(t) - q_j(t)\| \to 0, \quad (i, j \in N) \tag{11}$$

where R denotes the sensing radius, and D denotes the minimum distance for inter-collision avoidance.

Remark 3: *The objective (9) can preserve the connectivity with any splittings, and objective (10) can guarantee the collision avoidance among all agents, and the objective (11) can reach a velocity consensus for all agents.*

3 Adaptive dynamic interaction topology

Based on above-mentioned preliminaries, an adaptive dynamic interaction topology is proposed in this section, and the related framework and model are briefly demonstrated.

3.1 Following-interaction framework

The following-interaction framework composed of three key steps are devised by integrating four bio-inspired interaction mechanisms, as illustrated in Fig. 3.

Step1: The topological interaction is firstly employed to select all potential neighbors with a reasonably prescribed number, unlike the previous local interactions depend on an aprioristic assumption [29]. Therefore, topological interaction can be employed to shrink the number of neighbors in comparison to the traditional metric-distance interaction.

Step2: The visual interaction is devised to ensure the minimum number and optimal distribution of the neighborhood within local interaction. It consists two parts: (i) Due to the restrictions of the equipped sonars, the sensing field of UUV is limited. If this limited field is reasonably considered, it is an optimal strategy that the neighbor who is located in blindness zone is excluded to accomplish the local interaction. (ii) Due to the crowded phenomena existed in topological interaction, each individual has multiple nearest neighbors in a certain direction-interval. If one nearest neighbor who is located in each direction-interval, is selected to form a new neighborhood for each individual. Therefore, this step can further decrease the number and optimize the distribution of neighborhood after topological interaction.

Step3: The local following is essentially a non-average making-decision strategy integrated by single-nearest-neighbor and multiple-nearest-neighbors, rather than an average-velocity mechanism that is commonly assumed to design consensus or protocols. If the control parameter is smaller than an empirical triggered threshold, the SNNF originated from single-nearest-neighbor synergy is adopted to achieve a directed transmission of information, else the weighted-MNNF (WMNNF) originated from multiple-nearest-neighbors is proposed to synthesize all individual differences, in which a weight of each agent is determined by its corresponding interaction control parameter. In this step, advantages of the two following models are formulated in an unified framework, which can provide an adaptive making-decision to address behavior conflict and chain collision.

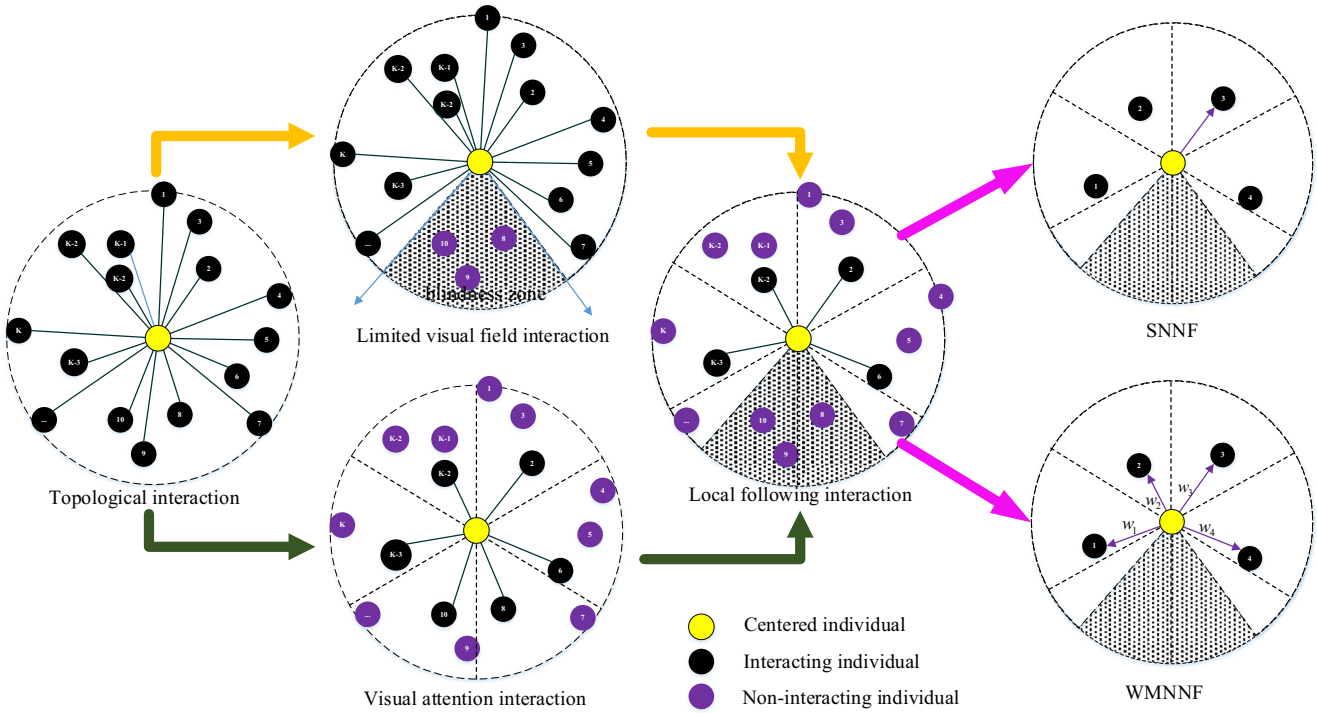

Fig. 3 Following-Interaction Framework. In this framework, the minimum number and optimal distribution of neighbors can be achieved through topological interaction and visual interaction, and the making-decision of individual behavior is adaptive and robust via SNNF and WMNNF. We use a yellow circle, black circle and purple circle to represent the centered individual, interacting individual and non-interacting individual, respectively. It is noted that the centered individual is only a simple reference individual in swarm, rather than a global centered agent in centralized control

3.2 Adaptive dynamic computing model

In terms of the proposed following-interaction framework, its corresponding computing model is developed in this subsection. Consider a group of N agents in the crowded UUV swarm, each individual has an omnidirectional view field with sensing radius R and blindness sectorω. The specific procedure is demonstrated as follows.

(i) Consider an omnidirectional view field of individual i, its neighbors set$N_i$at time t is determined by

$$N_i(t,\varphi) = \{j | d_{ij} \leq R_i, j \in \{1,\cdots,N\}, j \neq i\} \tag{12}$$

where ϕ denotes the view angle, and $N_i < N$.

Remark 4: *Eq. (12) is essentially a fixed distance interaction determined by sensing radius, and most of existing models all adopt this to decide the interaction intensity* [17–21].

(ii) The topological interaction is employed to select a fixed number with κ-nearest neighbors from N_i, determined by

$$N_i^1(t,\varphi,\kappa) = \underset{j\in N_i}{\operatorname{argmin}} \{j | d_{ij}(t)\} \tag{13}$$

where $N_i^1 < N_i$.

Remark 5: *Eq. (13) can decreases the number of neighbors in comparison to the fixed-distance interactions, such as Boids, Vicsek, and Couzin* [19].

(iii) The blindness angel ω is considered to improve the speed of information transmission via decreasing the omnidirectional view, which is consistent with the blindness sector caused by the restricted physical size [27]. Assuming the UUV is symmetrical about UUV heading, as shown in Fig. 4. Such that, the neighbor marked with the purple circle, who is located in the blindness sector, is excluded from interacting with others.

Hence, a new neighbor set N_i^2 with restricted blindness sector ω is determined by

$$N_i^2(t,\varphi,\kappa,\omega) = \{j | d_{ij}(t) \wedge \varphi_i - \omega_i, j \in N_i^1\} \tag{14}$$

where $N_i^2 < N_i^1$.

(iv) The individual i focuses on correlating and transmission of abnormal behaviors by utilizing the visual attention [37, 38], of which essence is that $\varphi_i - \omega_i$ is divided intom_c sectors along clockwise direction in the heading of agent i, then the nearest individual in each sub-sector is chosen, as shown in Fig. 5.

In particular, the view angle of each sub-sector of individual i is calculated as

$$\xi_{im} = \frac{\varphi_i - \omega_i}{m_c} \quad (m = 1,2,\cdots,m_c) \tag{15}$$

Then, the neighbor set Θ_i^m in m-th sub-sector is determined by

$$\Theta_i^m(t) = \{j | \xi_{im}(m-1) \leq \theta_{ij} - \vartheta_i \leq \xi_{im} m\} \tag{16}$$

where ϑ_i is the heading of individual i, and θ_{ij} is the azimuth of individual j relative to individual i. Such that the nearest neighbor in each sub-sector ℓ_i^m is chosen as

$$\ell_i^m(t) = \left\{ j | j = \underset{j\in\Theta_i^m}{\arg\min}\, d_{ij}, m = 1,2,\cdots,m_c \right\} \tag{17}$$

Finally, all the nearest individuals can generate a new neighbor set N_i^3, which is given by

$$N_i^3(t,\varphi,\kappa,\omega,m_c) = \{\ell_i^m(t), m = 1,2,\cdots,m_c\} \tag{18}$$

where $N_i^3 < N_i^2$.

Remark 6: *Eqs. (15) ~ (18) are essentially an optimal strategy to select the all candidate neighbors from N_i^2. The reasonable*

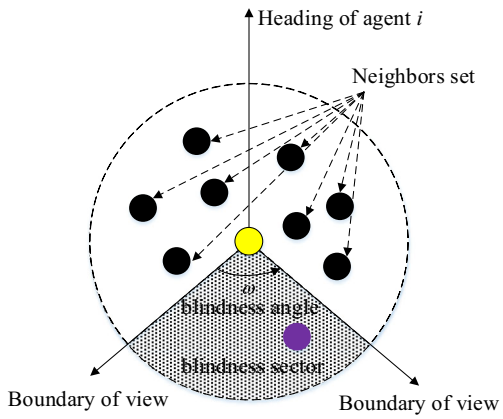

Fig. 4 Neighboring region of the agent i with a blindness angle

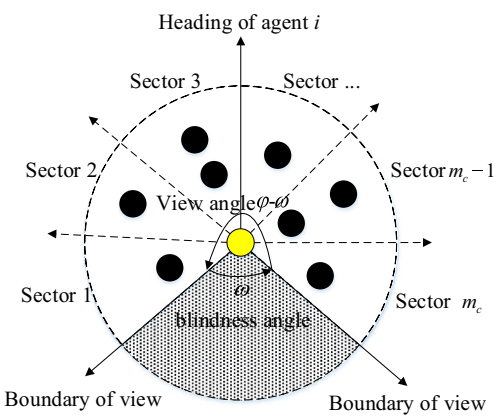

Fig. 5 Neighboring region of the individual i with divided sectors

number of sub-sectors and the choosing operation in each sub-sector can guarantee the only one agent existed in each sub-sector, which can address the crowded problem, and further avoid the behavior conflict and chain collision via *an optimal distribution in* N_i^3 .

(v) Based on N_i^3, an interaction control parameter $\delta_{ij}(t)$ is calculated by a synergy of position p_i, velocity q_i and heading ϑ_i to quantify the interaction intensity between individuals i and j [39]:

$$\delta_{ij}(t)=\frac{\alpha_{ij}}{1+\|p_i-p_j\|}\times\frac{\beta_{ij}\|\left(q_i-q_j\right)\times\overline{q}_i\|}{\sum_{j\in N_{i3}}\|\left(q_i-q_j\right)\times\overline{q}_i\|}\times\frac{\chi_{ij}}{1+\|\vartheta_i-\vartheta_j\|} \tag{19}$$

where α_{ij}, $\beta_{ij}$and χ_{ij} denote the coefficients corresponding with position, velocity and heading, respectively. And, $\overline{q}_i$ is an average-velocity of neighbor set $N_i^3(t)$.

Remark 7: *The* $\delta_{ij}(t)$ *is related to various factors such as relative distance, speed and heading between individuals, as well as the number of neighbors and spatial distribution. Furthermore, in the evolving process, swarm graph is dynamic, hence* $\delta_{ij}(t)$ *exhibits a time-varying characteristic.*

(vi) The SNNF and WMNNF by virtue of the proposed interaction control parameter $\delta_{ij}(t)$ are to design an adaptive following interaction model $u_i^f(t)$, which is given by

$$u_i^f(t)=\begin{cases}\sum_{j\in N_i^3}w_j u_j(t-\Delta t), & \delta_{ij}<\Delta_i\\ u_j(t-\Delta t), & \delta_{ij}\geq\Delta_i\end{cases} \tag{20}$$

where Δ_i is an empirical parameter, Δt denotes a sampling period, and w_j represents a weight with control law $u_i^f(t)$ of individual j. The w_j is given by

$$w_j(t)=\frac{u_j(t)}{\sum\limits_{j\in N_i^3}u_j(t)} \tag{21}$$

where $\sum\limits_{j\in N_i^3}w_j=1$, and $w_j(t)\geq 0$.

Remark 8: *If existing* $\delta_{ij}<\Delta_i$*, individual i adopts a WMNNF pattern. Conversely, if* $\delta_{ij}\geq\Delta_i$*, it adopts a SNNF pattern to follow* $j=\text{argmax}_{j\in N_i^3}\left\{\delta_{ij}|\delta_{ij}\geq\Delta_i\right\}$ *with the largest intensity.*

4 Self-organized cooperative control protocol

In this section, a novel self-organized cooperative control protocol is proposed, and its stability analysis is given to illustrate the feasibility and effectiveness.

4.1 Control protocol

The self-organized cooperative control protocol is derived from the proposed adaptive dynamic interaction topology and mathematics-based potential fields. In this approach, each UUV applies a control protocol that consists of four terms

$$u_i(t)=u_i^p+u_i^q+u_i^f+u_i^{dis},i=1,2,...,N \tag{22}$$

where u_i^p is the position coordination term, and u_i^q is the velocity consensus term, and u_i^f is the proposed following interaction term, andu_i^{dis} is the disturbance term.

(i) u_i^p is utilized to adjust the positions between individual i and its neighbors in N_i^3, which embodies the both attraction and repulsion rules [17]. It is given by the gradient-based potential fields as follows

$$u_i^p(t)=\sum_{j\in N_i^3}\psi_\alpha\left(\|p_i-p_j\|_\sigma\right)\sigma_\varepsilon\|p_i-p_j\|+\sum_{j\in N_i^3}\psi_\beta\left(\|p_i-p_j\|_\sigma\right)\sigma_\varepsilon\|p_i-p_j\| \tag{23}$$

where, ψ_α and ψ_β are the pairwise smooth attractive and repulsive potential functions, and $\|\cdot\|_\sigma$ is a σ-norm of a vector p_i-p_j, which is defined as

$$\|p_i-p_j\|_\sigma=(1/\varepsilon)\left[\sqrt{1+\varepsilon\|p_i-p_j\|^2}-1\right] \tag{24}$$

where $\varepsilon\in(0,1)$ is a fixed parameter. The gradient of $\|p_i-p_j\|_\sigma$ defined by $\sigma_\varepsilon\|p_i-p_j\|$ is given by

$$\begin{aligned}\sigma_\varepsilon\|p_i-p_j\|=\nabla\|p_i-p_j\|_\sigma&=\frac{\|p_i-p_j\|}{\sqrt{1+\varepsilon\|p_i-p_j\|^2}}\\&=\frac{\|p_i-p_j\|}{1+\varepsilon\|p_i-p_j\|_\sigma}\end{aligned} \tag{25}$$

where ∇ denotes a gradient operator.

Due to the limited forces provided by actuators, both ψ_α and ψ_β triggered by two continuously bounded active functions Θ_α and Θ_β, are designed to generate repulsive and attractive forces of all agents. Specifically, the repulsive function and its corresponding active function are given by

$$\psi_\alpha(d_{ij})=\int_{\|R\|_\sigma}^{d_{ij}}\Theta_\alpha(s)ds \tag{26}$$

$$\Theta_\alpha(d_{ij})=\begin{cases}-\varpi_\alpha/d_{ij}^2, & d_{ij}\in[0,\|R\|_\sigma)\\ 0, & d_{ij}\in[\|R\|_\sigma,+\infty)\end{cases} \tag{27}$$

where $\varpi_\alpha>0$ is a designing parameter.

Similarly, the attractive function and its corresponding active function are given by

$$\psi_\beta(d_{ij}) = \int_0^{d_{ij}} \Theta_\beta(s)ds \tag{28}$$

$$\Theta_\beta(d_{ij}) = \begin{cases} \dfrac{-\varpi_\beta(d_{ij}-d_{\min})(d_{ij}-\|R\|_\sigma)}{d_{ij}}, & d_{ij}\in[0,\|R\|_\sigma) \\ 0, & d_{ij}\in[\|R\|_\sigma,+\infty) \end{cases} \tag{29}$$

where $\varpi_\beta > 0$ is a designing parameter, and $d_{\min}$ represents the minimum local distance.

Hence, the total potential functions for the crowded UUV swarm are given by

$$V(p,q) = \frac{1}{2}\sum_i \sum_{j\neq i} \psi_{ij}\left(\|p_i-p_j\|_\sigma\right) \tag{30}$$

where $\psi_{ij} = \psi_\alpha + \psi_\beta$.

To simplify the presentation, (23) can be given by

$$u_i^p(t) = \sum_{j\in N_i^3} \nabla_{p_i}\psi_{ij}\left(\|p_i-p_j\|_\sigma\right) \tag{31}$$

(ii) u_i^q represents the velocity alignment using consensus-based protocol

$$u_i^q(t) = \sum_{j\in N_i^3} a_{ij}(q)\left(q_j-q_i\right) \tag{32}$$

where $a_{ij} > 0$ is an element of adjacency matrix.

(iii) u_i^f represents the proposed following interaction, which is utilized to control individuals tracking the informed agent and make the velocity consensus. Its expression is of form as

$$u_i^f(t) = \begin{cases} \sum_{j\in N_i^3} w_j\left(\nabla_{p_i}\psi_{ij}(\|p_i-p_i\|_\sigma) + \lambda_1 a_{ij}\left(q_i-q_j\right)\right), & \delta_{ij} < \Delta_i \\ \lambda_{2i}\nabla_{p_i}\psi_{ij}\left(\|p_i-p_j\|\right) + \lambda_2 a_{ij}\left(q_i-q_j\right), & \delta_{ij}\geq\Delta_i \end{cases} \tag{33}$$

where Δ_i is an empirical parameter determined by

$$\Delta_i = \exp(-\lambda\cdot\Phi_i^2) \tag{34}$$

$$\Phi_i = \frac{1}{|N_i|+1}\left\|\sum_{j\in N_i^3\cup i}, \frac{q_j}{\|q_j\|}\right\| \tag{35}$$

where is positive constant. Moreover, λ_{2i} and λ_2 are feedback gain coefficients, where λ_{2i} is given by

$$\lambda_{2i} = \begin{cases} \Upsilon_q, & \|q_i\|\leq V_{\max} \\ \dfrac{\Upsilon_q\Upsilon_m}{\|q_i\|+\Upsilon_m-V_{\max}}, & \|q_i\| > V_{\max} \end{cases} \tag{36}$$

where Υ_q and Υ_m are positive constants, and $V_{\max}$ is the maximum velocity given by Eq. (8).

(iv) u_i^{dis} describes a composing of external disturbances and noises, which is given by

$$\dot{u}_i^{dis}(t) + T_d u_i^{dis}(t) = K_d F_d \tag{37}$$

where T_d denotes constant matrix,K_d denotes gain matrix, and F_d denotes the largest amplitude of the white noise. It should be noted that u_i^{dis} is continuous and bounded.

Remark 9: *In control protocol Eq. (22), the individual characteristics represented by w_j can generate an influence on forming the neighbor set $N_i^3(t,\psi,k,\omega,m_c)$, which is not similar to the existing models that all individuals are assumed to be an equal state. Thus, the proposed control protocol is a more realistic model.*

Remark 10: *In control protocol Eq. (22), each individual in neighbors set is updated within each sampling period, rather than just tracking a fixed target to follow. Therefore, it is essentially different from the leader-following control protocol* [9].

Remark 11: *In control protocol Eq. (22), if existing $\delta_{ij} < \Delta_i, u_i^f$ is determined by its all neighbors. if existing $\delta_{ij}\geq\Delta_i, u_i^f$ is determined by the individual with largest interaction intensity. Thus, the control protocol in* [40] *can be regarded as a special case of our proposed control protocol.*

Assumption 2: *In the G associated with $N_i^3(t,\psi,k,\omega,m_c)$, there exists a directed path from the informed agent to any other agent.*

4.2 Stability analysis

Theorem 1: *Consider a crowded UUV swarm with dynamic model (1), if the initial graph G(0) is connected and initial state is from the LaSalle invariance principle, and Assumption 2 holds, such that all agents can achieve a self-organized cooperative control consensus under the proposed control protocol (22) ~ (37). Then, following statements hold:*

i) *The velocities of all individuals will asymptotically converge to a consensus.*

ii) *Almost every final configuration reaches in a local minimum.*
iii) *No collisions occur for all* $t \geq 0$.
iv) *No splittings occur for all* $t \geq 0$.

Proof Consider a Lyapunov-like energy function under $\delta_{ij} < \Delta_i$

$$Q(p,q) = \frac{1}{2}\sum_{i=1}^{N}\left(U(p) + \left(q_i - q_j\right)^T\left(q_i - q_j\right)\right) \tag{38}$$

where

$$U(p) = V(p,q) + w_j \sum_{j=N_i^3} \psi_{ij}\left(\left\|p_i - p_j\right\|_\sigma\right) \tag{39}$$

Substituting (30) into (39), we can obtain

$$U(p) = \left(1 + w_j\right) \sum_{j=N_i^3} \psi_{ij}\left(\left\|p_i - p_j\right\|_\sigma\right) \tag{40}$$

Let (p_c, q_c) be the center of mass (COM) of neighbour set, which is given by

$$p_c = \frac{1}{\mathcal{N}}\sum_{i=1}^{\mathcal{N}} p_i, q_c = \frac{1}{\mathcal{N}}\sum_{i=1}^{\mathcal{N}} q_i \tag{41}$$

where $\mathcal{N} = N_i^3(t)$ is of convenience.

Let $\widetilde{p}_i = p_i - p_c$ and $\widetilde{q}_i = q_i - q_c$ describe the relative positions and velocities between agent i and (p_c, q_c), then $p_i - p_j = \widetilde{p}_i - \widetilde{p}_j = \widetilde{p}_{ij}, q_i - q_j = \widetilde{q}_i - \widetilde{q}_j = \widetilde{q}_{ij}$, and $u_i^p(t)$ can be now written as

$$u_i(t) = -\left(1 + w_j\right) \sum_{j\in\mathcal{N}} \nabla_{p_i}\psi_{ij}\left(\left\|\widetilde{p}_{ij}\right\|_\sigma\right) - a_{ij}\widetilde{q}_{ij} - \lambda_1 w_j \sum_{j\in\mathcal{N}} a_{ij}\widetilde{q}_{ij} \tag{42}$$

Then (38) is rewritten as

$$Q\left(\widetilde{p},\widetilde{q}\right) = \frac{1}{2}\sum_{i=1}^{\mathcal{N}}\left(\left(1 + w_i\right) \sum_{j\in\mathcal{N}} \psi_{ij}\left(\left\|\widetilde{p}_{ij}\right\|_\sigma + \widetilde{q}_{ij}^{\ T}\widetilde{q}_{ij}\right)\right. \tag{43}$$

According to the symmetry of ψ_{ij} and the symmetric matrices of a_{ij}, then

$$\frac{\partial\psi_{ij}\left(\left\|\widetilde{p}_{ij}\right\|_\sigma\right)}{\partial\widetilde{p}_{ij}} = \frac{\partial\psi_{ij}\left(\left\|\widetilde{p}_{ij}\right\|_\sigma\right)}{\partial\widetilde{p}_i} = -\frac{\partial\psi_{ij}\left(\left\|\widetilde{p}_{ij}\right\|_\sigma\right)}{\partial\widetilde{p}_j} \tag{44}$$

Differentiating (43) gives

$$\dot{Q}\left(\widetilde{p},\widetilde{q}\right) = \left(1 + w_i\right)\sum_{i=1}^{\mathcal{N}} \nabla_{\widetilde{p}_{ij}}\left(\sum_{j\in\mathcal{N}} \dot{\psi}_{ij}\left(\left\|\widetilde{p}_{ij}\right\|_\sigma\right)\right)^{\mathrm{T}}\widetilde{q}_{ij} + \widetilde{q}_{ij}^{\ T}u_i \tag{45}$$

Substituting (42) into (45), we have

$$\begin{aligned}\dot{Q}\left(\widetilde{p},\widetilde{q}\right) &= \left(1 + w_i\right)\sum_{i=1}^{\mathcal{N}} \nabla_{\widetilde{p}_{ij}}\left(\sum_{j\in\mathcal{N}} \dot{\psi}_{ij}\left(\left\|\widetilde{p}_{ij}\right\|_\sigma\right)\right)^{\mathrm{T}}\widetilde{q}_{ij} + \sum_{i=1}^{\mathcal{N}}\widetilde{q}_{ij}^{\ T}\left[-\left(1 + w_j\right)\sum_{j\in\mathcal{N}}\nabla_{p_i}\psi_{ij}\left(\left\|\widetilde{p}_{ij}\right\|_\sigma\right) - a_{ij}\widetilde{q}_{ij} - \lambda_1 w_j\sum_{j\in\mathcal{N}} a_{ij}\widetilde{q}_{ij}\right] \\ &= \sum_{i=1}^{\mathcal{N}}\widetilde{q}_{ij}^{\ T}\left(-a_{ij}\widetilde{q}_{ij} - \lambda_1 w_j\sum_{j\in\mathcal{N}} a_{ij}\widetilde{q}_{ij}\right) = -\widetilde{q}^T\left[L\left(\widetilde{p}\right) + a_{ij}I_{\mathcal{N}}\otimes I_n\right]\widetilde{q}^T\end{aligned} \tag{46}$$

where $\widetilde{p} = \mathrm{col}[p_1, p_2, p_{\mathcal{N}}]^T \in \mathbb{R}^{\mathcal{N}\times n}$, $\widetilde{q} = \mathrm{col}[q_1, q_2, q_{\mathcal{N}}]^T \in \mathbb{R}^{\mathcal{N}\times n}$, $\otimes$ is the Kronecker operator, $L(\widetilde{p})$ is the Laplacian matrix of $G(\widetilde{p})$, and $I_{\mathcal{N}}$ denotes a $\mathcal{N}$ dimensional unit vector. Due to the existing $a_{ij} \in [0, 1]$, we can obtain

$$\dot{Q}\left(\widetilde{p},\widetilde{q}\right) = -\widetilde{q}^T\left[L\left(\widetilde{p}\right) + a_{ij}I_{\mathcal{N}}\otimes I_n\right]\widetilde{q}^T \leq 0 \tag{47}$$

Thus, by virtual of Barbalat Lemma, it holds that

$$\lim_{t\to\infty}\dot{Q}\left(\widetilde{p},\widetilde{q}\right) = 0 \tag{48}$$

It is implied that $Q(\widetilde{p},\widetilde{q})$ is monotonic in (48). Let $\Omega_c = \{(p,q) : Q(p,q) \leq Q_0\}$ is a compact set, existing $Q_0(p_0, q_0) = \psi_\sigma(0) > 0$ is the initial energy. Moreover, it is easy to obtain that $Q(\widetilde{p},\widetilde{q}) \leq Q_0$ is closed and bounded for any time internal $t \in [0, t^*]$. Therefore, the control system is asymptotically stable.

From the LaSalle invariance principle, all solutions $(\widetilde{p},\widetilde{q})$ of Eq. (22) starting in $\Omega_c$coverage to its largest invariant set given by

$$S = \left\{\left(\widetilde{p},\widetilde{q}\right) \in \mathbb{R}^{\mathcal{N}\times n} : \dot{Q}(p,q) = 0\right\} \tag{49}$$

It can be evident that $\dot{Q}(\widetilde{p},\widetilde{q}) = 0$ and $\widetilde{q} = 0$, and we can deduce that velocities of all agents asymptotically match each other, i.e.,

$$q_1 = q_2 = \cdots = q_{\mathcal{N}} \tag{50}$$

Now, part i) and ii) have been proved. Subsequently, we prove part iii) by contradiction strategy. Assume existing an instant time $t = t_1 > 0$, two individuals k and l collide, i.e., $\|p_l(t_1) - p_k(t_1)\| \le D$, where D is the minimum distance between two agents. For all $t > 0$, we obtain a smooth potential function,

$$\begin{aligned} Q(p(t_1)) &= \frac{1}{2}\sum_i \sum_{j\neq i} \psi_\sigma\left(\|p_i - p_j\|_\sigma\right) = \psi_\sigma\left(\|p_l(t_1) - p_k(t_1)\|_\sigma\right) \\ &+ \frac{1}{2}\sum_{i\in\mathcal{N}\setminus\{k,l\}} \sum_{j\in\mathcal{N}\setminus\{i,k,l\}} \psi_\sigma\left(\|p_i(t_1) - p_j(t_1)\|_\sigma\right) \\ &\ge \psi_\sigma\left(\|p_l(t_1) - p_k(t_1)\|_\sigma\right) \end{aligned} \tag{51}$$

Hence, existing $Q(p(t_1)) \ge \psi_\sigma(0) = Q_0$. However, it is in contradiction with an inequality

$$Q(p(t_1)) \le Q_0 \tag{52}$$

Therefore, in terms of (51) and (52) in contradiction with the invariant principle, no two agents collide at any time $t \ge 0$.

Furthermore, assume that $G(t)$ switches at time $t_k, k = 1, 2, \cdots$, and $G(t)$ is a fixed graph on each time-interval $[t_{k-1}, t_k]$. Note that Q_0 is finite and the time derivative of $Q(t)$ in $t \in [t_0, t_1]$ is (47), existing an inequality

$$Q(t_1) \le Q_0 < \infty, \forall t \in [t_0, t_1) \tag{53}$$

Such that

$$\lim_{d_{ij}\to R} \psi(d_{ij}) = \infty \tag{54}$$

Clearly, it is implied that there is no edges will be lost before t_1 and be added at switching t_1. Similar to the $t \in [t_0, t_1]$, time derivative $Q(t)$ on each time-interval $[t_{k-1}, t_k]$, is also satisfied with (47). It can be given by

$$Q(t_k) \le Q(t_{k-1}) \le Q_0 < \infty, \forall t \in [t_{k-1}, t_k), k = 1, 2\cdots \tag{55}$$

Thus no edges will be lost before t_k and be added at switching t_k. In addition, by virtue of the Assumption 2, $G(t)$ can be guaranteed to keep connectivity for all $t \ge 0$.

From the above proof, we can conclude that each agent in swarm can asymptotically converge to a consensus, and no collisions and splittings occur between any two agents. □.

Remark 12: *For case of $\delta_{ij} \ge \Delta_i$, its stability proof is similar to the case of $\delta_{ij} < \Delta_i$. Due to space limitations, a more rigorous proof is omitted herein.*

5 Simulation results

In this section, we will provide simulation results to demonstrate effectiveness and robustness of our proposed approach. We consider a crowed UUV swarm with $N = 51$. The initial positions are located in 50×50 m such that the initial graph is connected, and initial headings and velocities are chosen from $[-\pi, \pi]$ rad and $[0, 10]$m/s, respectively. Without the loss of generality, the heading of each agent specifies the direction of velocity, and $V_{\max} = 15m/s$. The nonlinear UUV model can be seen in [27]. The following parameters remain fixed through all simulations: $\phi = 2\pi$, $\omega = [-\pi/6, \pi/6]$, $m_c = 12$, $\kappa = 8$, $\alpha_{ij} = 1.2$, $\beta_{ij} = 1.2$, $\chi_{ij} = 1.2$, $\varpi_\alpha = 100$, $R = 12m$, $\varpi_\beta > 100$, $d_{\min} = 4m$, $\varepsilon = 0.5$, $= 0.5$, $\Upsilon_q = 1$, $\Upsilon_m = 0.2$, $T_d = diag\,[100, 100, 100]$, $K_d = diag\,[10, 5, 6]$, $F_d = 1$, and $D = 0.5m$.

All experiments are divided into two cases: without external stimuli signal and with external stimuli signal, which are conducted in MATLAB and C++ Platform. In addition, a computer with Intel(R) Core™i7 CPU3.20GHz is utilized for simulations.

5.1 Self-organized cooperative control without external stimuli signal

In the absence of external stimuli signal, assuming that a crowded UUV swarm performs a desired velocity $[5, 5]^T$ m/s. The experimental results are demonstrated to prove the asymptotic convergence of the proposed self-organized cooperative control in Figs.6, 7 and 8.

Figure 6 exhibits the flocking trajectories without external stimuli signal. Fig. 6a shows the initial pattern, in which each individual is marked by green circle with arrow, and the scale of arrow denotes the magnitude of initial velocity. Fig. 6b shows the path trajectories, it is clearly observed that the swarm can be self-organized to achieve the asymptotic convergence. Moreover, consensus and synchronicity can be simultaneously guaranteed as shown in Fig. 6c, in which all velocities are equal to $[5, 5]^T$. Fig. 6d plots the relative distance d_{ij} of crowded UUV swarm, and d_{ij} satisfies $D \le d_{ij} \le R$. Hence, we can deduce a conclusion that without any collisions and splits occurring in self-organized motion.

Figure 7 plots velocities of all individuals including velocity-x and velocity-y, respectively. Due to great convergence of the proposed consensus, these velocities can be quickly converged at $t = 10$s, and flocking swarm can be synchronous to the desired velocity $[5, 5]^T$ at $t = 50$s. Additionally, one can be seen that the crowded swarm can keep a relatively stable distance without a larger change after $t = 10$s in Fig. 8. From all above results, all observations are in close agreement with our theoretical predictions, and it is implied that our approach can achieve a self-organized flocking without triggering any conflict and collision.

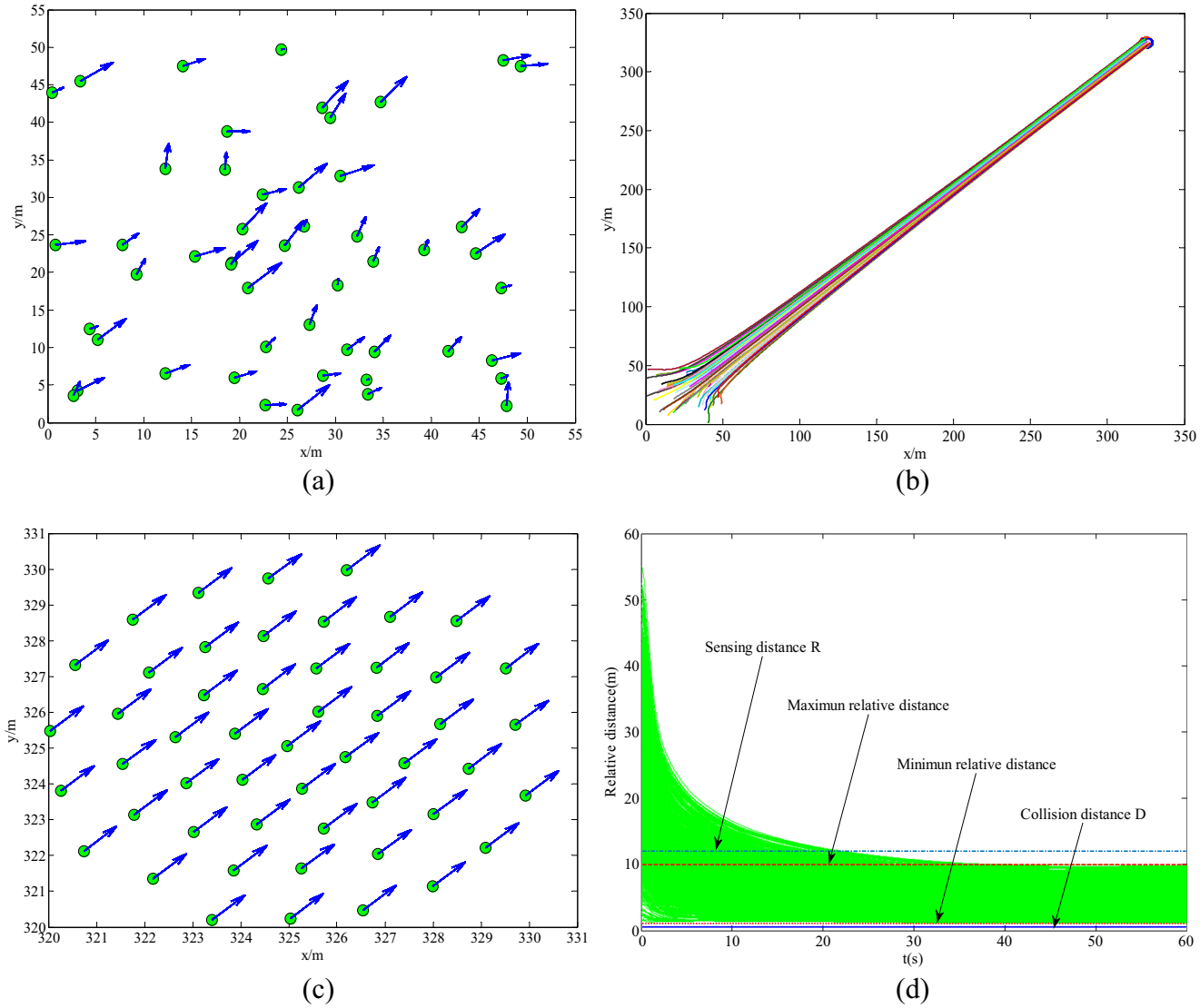

Fig. 6 Flocking without external stimuli signal: (**a**) Initial pattern, (**b**) path trajectory, (**c**) final pattern and (**d**) relative distance

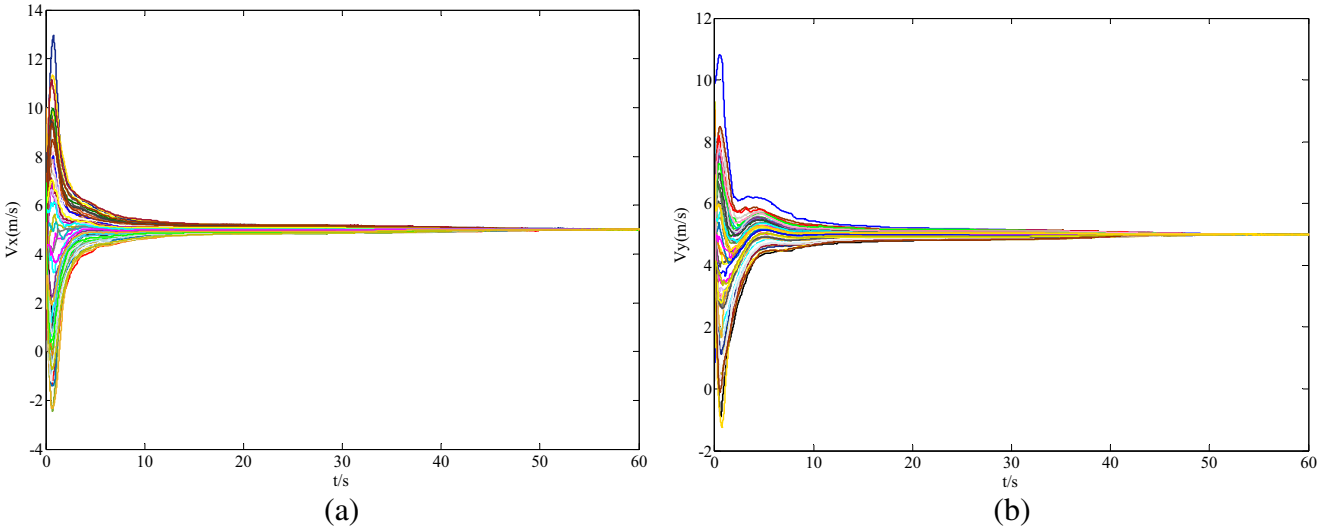

Fig. 7 The velocities of all individuals at $t = 60$s. (**a**) velocity-x and (**b**) velocity-y

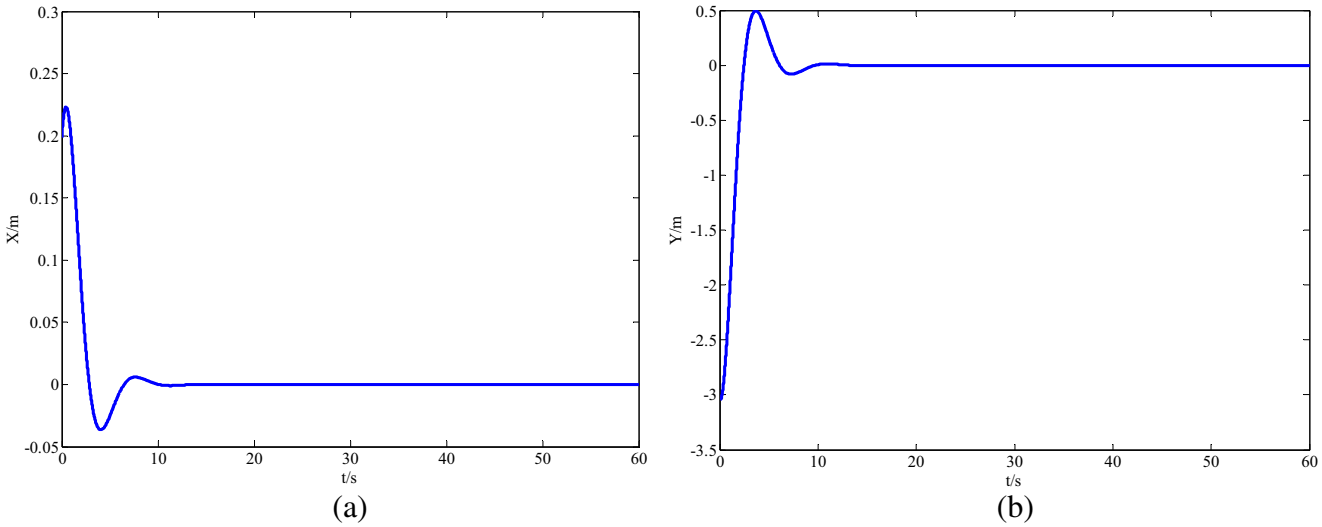

Fig. 8 The average position error of all individuals at $t = 60$s. (**a**) position-x average error and (**b**) position-y average error

5.2 Self-organized cooperative control with external stimuli signal

In the presence of an external stimuli signal, assuming that the crowded UUV swarm performs a desired velocity $[5, 5]^T$ m/s, and an informed agent who moves on boundary of swarm changes its heading in responding to the stimuli signal, which is given by

$$u_i^s(t) = \hbar\left(q_i - q_i^s\right) \tag{56}$$

where $\hbar = 10$ denotes the feedback gain, and $q_i^s = [5, 0]^T$ is an expected velocity of agent i who is labeled as informed agent.

In order to verify the efficiency of our proposed control approach, self-organized fission/fusion method (SFF) [39] and single-informed-based distributed consensus (SDC) [40] are employed to perform the comparative experiments. The differences between the three methods are the neighbor number and following mechanism. It is noted that the external stimuli signal appears at $t = 60$s after flocking achieved, and comparison results are illustrated in Figs. 9, 10 and 11 and Table 1.

Figures 9, 10 and 11 present the results of comparisons among SFF, SDC and our proposed approach in the presence of an external stimuli signal, respectively. The Figs. 9a, 10a and 11a exhibit flocking trajectories, and Figs. 9b, 10b and 11b show their final patterns, respectively, in which the agent marked with red circle indicates an informed agent and the dotted line indicates its trajectory after $t = 60$s. The informed agent changes its heading from $[5, 5]^T$ to $[5, 0]^T$ at $t = 60$s, and its neighbors can synchronously change their original heading in Fig. 9. However, all neighbors eventually fail to track the informed agent, which leads to a splitting swarm into two sub-groups. The one sub-group is composed of the only informed agent who tracks the stimuli signal, and the other sub-group consisting 50 individuals moves in a direction between $[5, 5]^T$ and $[5, 0]^T$. The similar results are provided in Fig. 10, where the swarm is also separated into two sub-groups. The only difference between Figs. 9 and 10 is that the direction of SDC with respect to the informed agent is smaller than that of SFF. The best performance of our proposed approach can be seen in Fig. 11, in which all neighbors accurately follow the informed agent and the velocity consensus can be guaranteed, such that the flocking pattern remains stable.

Additionally, the relative distances among crowded UUV swarm are considered after external stimuli signal appearing at $t = 60$s, as shown in Table 1. It is observed that the minimum and maximum relative distance d_{ij} of our proposed consensus are 1.1845 m and 11.9813 m, respectively, both of which satisfy $D \leq d_{ij} \leq R$, such that the objectives (9) and (10) can be guaranteed without any splits and collisions even under a stimuli signal. Furthermore, the minimum relative distances of other approaches are larger than the predefined collision distance $D = 0.5m$. Thus, the SFF and SDC can also achieve the avoiding collisions. However, maximum relative distances, 54.6522 m and 23.4991 m, are larger than the predefined sensing distance $R = 12m$, which indicates that communicating connections of SFF and SDC are broken due to splits occurring. Obviously, it is evident that our approach is more robust against fluctuations and disturbances in comparison to other approaches.

Table 1 Comparisons of relative distances (The optimal result is in bold)

Control approach	Minimum distance (m)	Maximum distance (m)
SFF	1.3828	54.6522
SDC	1.3427	23.4991
Proposed consensus	**1.1845**	**11.9813**

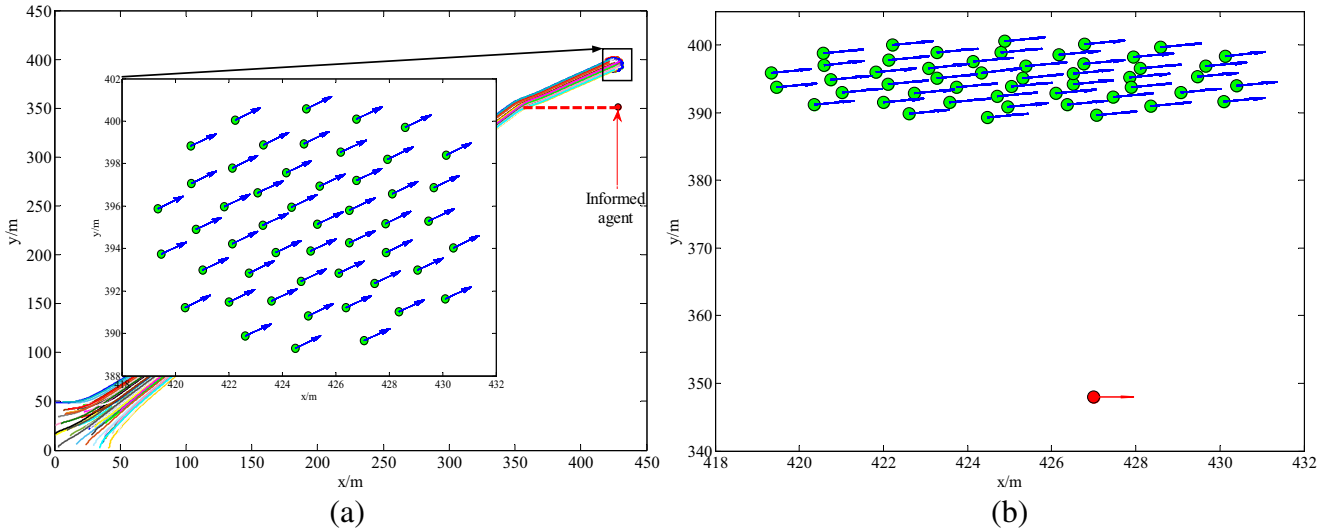

Fig. 9 The results of SFF under an external stimuli signal. (**a**) Flocking trajectory and (**b**) Final pattern

The reason why these differences are due to different the following mechanisms existed in the three approaches. Clearly, both the SFF and SDC employ the average mechanism, in which two limitations are exposed. (i) All individuals within sensing range are automatically activated to participate in local interaction, where how to optimize information transmission and computing is not fully considered. (ii) The averaged-synergy filters or dilutes the external stimuli signals, such that all heterogeneous propensities and their effects may be ignored. Conversely, our proposed approach can alleviate the above two limitations from two aspects. (i) Our following-interaction framework can ensure the minimum number and optimal distribution of neighborhood. (ii) Our adaptive computing strategy considers all individual differences via single-nearest-neighbor and multiple-nearest-neighbors synergies with nonlinear weights.

5.3 Discussion

In order to further verify the robustness of our proposed approach, three quantitative indicators such as mean heading (MH), orderness parameter (OP) and scale parameter (SP) are devised to demonstrate the comparative performances.

The MH is defined as

$$\varphi_{MH}(t) = \frac{1}{N}\left|\sum_{i=1}^{N}, e^{j\vartheta_i}\right| \tag{57}$$

where N represents the swarm size. Generally, a great $\varphi_{MH}(t)$ value shows a worse flocking.

The OP is defined as:

$$\varphi_{OP} = \frac{1}{N}\left|\sum_{i=1}^{N}, \frac{q_i}{\|q_i\|}\right| \tag{58}$$

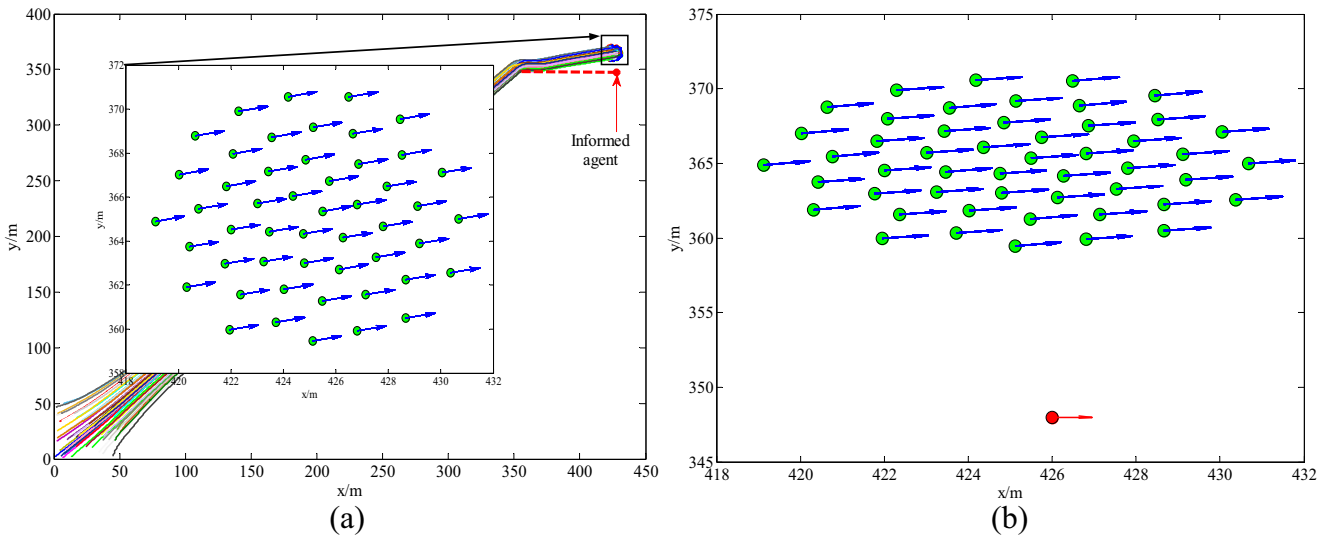

Fig. 10 The results of SDC under an external stimuli signal. (**a**) Flocking trajectory and (**b**) Final pattern

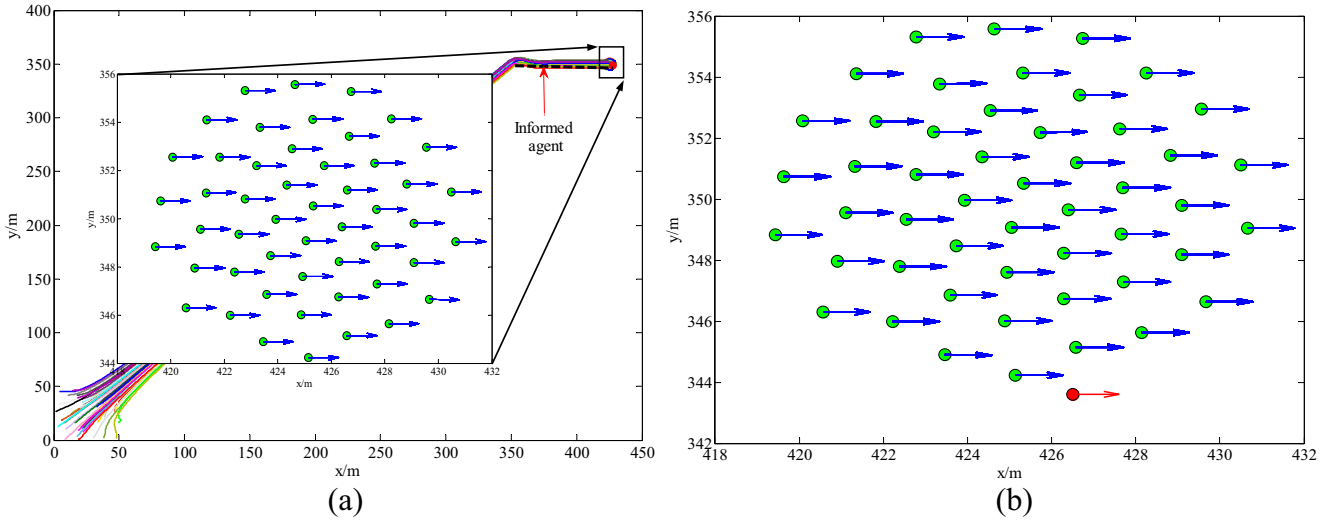

Fig. 11 The results of our approach under an external stimuli signal. (**a**) Flocking trajectory and (**b**) Final pattern

where $\|q_i\|$ represents the Euclidean norm of velocity vector of agent i. Apparently,$\varphi_{OP} \in [0, 1]$, the swarm is orderness if $\varphi_{OP} = 1$. Conversely, it is unordered when$\varphi_{OP} = 0$.

The SP is defined as

$$\varphi_{SP} = \sqrt{\frac{1}{N}\sum_{i=1}^{N} \|p_i - p_c\|^2} \tag{59}$$

where p_c represents the COM given by Eq. (41). Obviously, a smaller φ_{SP} indicates a more cohesive distribution.

In particular, all simulations are repeated 50 times, and the results are demonstrated in Fig. 12.

Figure 12a demonstrates curves of MH results. At $t = 0$, all results obtained from three approaches are divergent. At $t =$ 10s, the values asymptotically converge to a constant due to desired head $[5, 5]^T$ followed by all UUVs. When an external stimuli signal $q_i^s = [5, 0]^T$ appears $t = 60$s, this indicator significantly declines and slightly converges to its minimum at $t = 65$ s. Although SFF and SDC complete flocking, only our approach can simultaneously guarantee flocking and following behaviors. Therefore, it is implied that the tracking and synchronizing capabilities of our approach outperform SFF and SDC.

As shown in Fig. 12b, the OP result of our approach is sensitive to internal and external disturbances in comparison to other approaches, and greater convergence speed can be obtained to form an ordered flocking, which can be seen when the internal and external disturbances appear at $t = 0$ and $t =$ 60s, respectively. Additionally, the OP result of our approach eventually converges to 1, which is higher than that of SFF and SDC. The reasons accounting for this result are insufficient information interactions and long convergence time in SFF and SDC. Consequently, it is implied that our approach has an excellent orderness.

Figure 12c illustrates SP results. In initial stage, there exists a fluctuation. After $t = 10$s, SP results gradually converge. Obviously, this indicator monotonously increases when individuals response to the external stimuli signal, and our approach is better than that of other two methods. The reason why these results occur is that there is no splits in our approach, but other two approaches separate the swarm into two sub-groups. Accordingly, it is clear that our designed approach is effective for UUV swarm in the presence of external stimuli signal.

Summarily, it is clear that our proposed control approach shows better robustness against fluctuations and disturbances in comparison to the SFF and SDC. It is also confirmed that the minimum number and optimal distribution of neighborhood can improve the speed of information dissemination in local interaction. Furthermore, the proposed approach can effectively achieve the swarm cohesion and collision avoidance.

6 Conclusions

In this paper, a novel bio-inspired self-organized cooperative control is developed to address behavior conflict and chain collision for crowded UUV swarm in the presence of fluctuations and disturbances. All simulation results prove that our proposed approach can obtain robust control performance without any collision and split occurring, in comparison to the existing methods via MH, OP and SP indicators. The primary contributions of this paper are summarized as follows:

(i) An optimized following interaction framework is devised by the topological interaction and visual interaction to improve the synchronous velocities and save the sensing

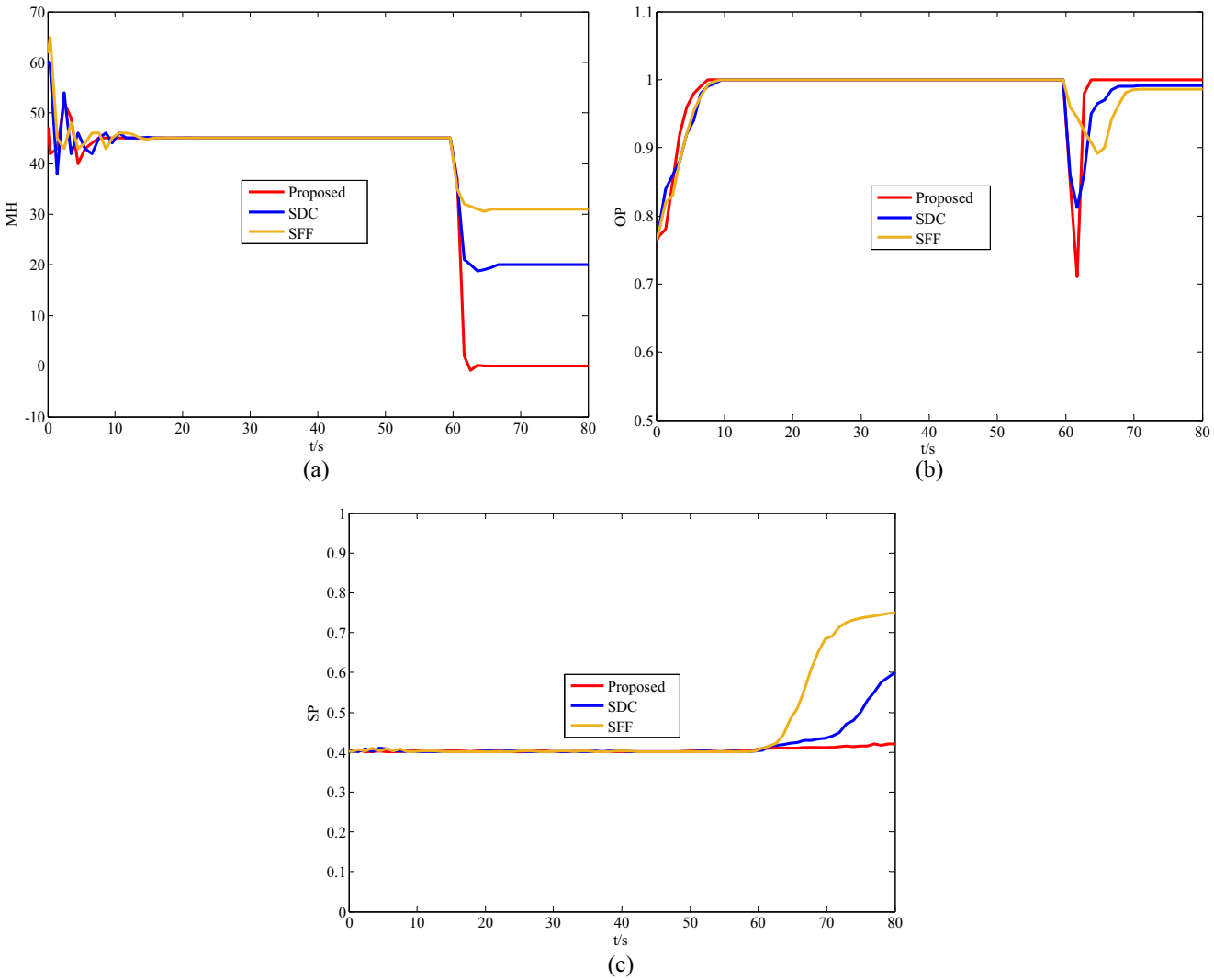

Fig. 12 Comparison results of three approaches: (**a**) MH, (**b**) OP and (**c**) SP

costs, in which two constrains, i.e., limited view and crowded phenomenon, are simultaneously considered. This framework can ensure the minimum number and optimal distribution of the neighborhood for each agent in dynamic graph, instead of the previous fixed-number and fixed-distance studies.

(ii) An adaptive dynamic computing model is proposed by incorporating SNNF and WMNNF to establish an effective decision-making strategy for solving the problems of behavior conflict and chain collision, where the influence of each individual on sensitive behavior is synthesized by a nonlinear weight. Therefore, it is essentially a non-average mechanism unlike the traditional average-velocity mechanism.

(iii) By virtue of adaptive dynamic interaction topology, a cooperative control protocol based on the proposed following model and mathematics-based potential fields is designed to steer a self-organized flocking with two abilities of the connectivity-preserving and collision-avoiding. Furthermore, the sufficient condition is analyzed via Laypunov and LaSalle invariance principle. It is confirmed that our approach can be suitable for cooperative control of crowded UUV swarm.

For future works, the jointed effects of time delays and packet loss will be considered in this self-organized cooperative control approach, and the control performance can be further improved towards achieving the lager-scale heterogeneous UUV swarm.

Acknowledgments The authors acknowledge the financial support from the National Natural Science Foundation of China under Grant 11404205, Natural Science Foundation of Shaanxi under Grant 2019JQ-026 and Fundamental Research Funds for Central Universities under Grant GK201903016 and GK201803023. And the authors would like to thank all reviewers and editors who provided extensive valuable feedback.

Compliance with ethical standards

Conflict of interest This work is original research and approved by all authors. The authors declare that they have no conflict of interest.

References

1. Wu Y, Low KH, Lv C (2020) Cooperative Path Planning for Heterogeneous Unmanned Vehicles in a Search-and-Track Mission Aiming at an Underwater Target. IEEE Trans Veh Technol 69(6):6782–6787
2. Londhe PS, Patre BM (2019) Adaptive fuzzy sliding mode control for robust trajectory tracking control of an autonomous underwater vehicle. Intell Serv Robot 12:87–102
3. Ingrand F, Ghallab M (2017) Deliberation for autonomous robots: a survey. Artif Intell 247:10–14
4. Bukhari AC, Kim YG (2013) A research on an intelligent multi-purpose fuzzy semantic enhanced 3D virtual reality simulator for complex maritime missions. Appl Intell 38:193–209
5. Liang HT, Qiang N (2020) Distributed Cooperative Control Based on Dynamic Following Interaction Mechanism for UUV Swarm. 2020 39th Chinese control conference (CCC), Shenyang, China, pp 5092–5097
6. Oh H, Shirazi AR, Sun CL, Jin YC (2017) Bio-inspired self-organising multi-robot pattern formation: a review. Robot Auton Syst 91:83–100
7. Ferrante E, Turgut AE, Huepe C, Stranieri A, Pinciroli C, Dorigo M (2012) Self-organized flocking with a mobile robot swarm: a novel motion control method. Adapt Behav 20(6):460–477
8. Pandey P, Pompili D, Yi J (2015) Dynamic collaboration between networked robots and clouds in resource-constrained environments. IEEE Trans Autom Sci Eng 12(2):471–480
9. Wang J, Wang C, Wei Y, Zhang C (2020) Neuroadaptive sliding mode formation control of autonomous underwater vehicles with uncertain dynamics. IEEE Syst J 14(3):3325–3333
10. Sahu BK, Subudhi B (2018) Flocking Control of Multiple AUVs Based on Fuzzy Potential Functions. IEEE Trans Fuzzy Syst 26(5): 2539–2551
11. Yang H, Zhang F (2012) Robust control of formation dynamics for autonomous underwater vehicles in horizontal plane. J Dyn Syst Meas Control 134:031009
12. Pan W, Jiang D, Pang Y, Qi Y, Luo D. Distributed Formation Control of Autonomous Underwater Vehicles Based on Flocking and Consensus Algorithms. In: Huang Y, Wu H, Liu H, Yin Z (eds) Intelligent robotics and applications. ICIRA 2017. Lecture Notes in Computer Science, vol 10462. Springer, Cham. https://doi.org/10.1007/978-3-319-65289-4_68
13. Chen YY, Zhu DQ (2020) Research on the Method of Multi-AUV Formation Control Based on Self-organized Artificial Potential Filed. Control Eng China 26(10):1875–1881
14. Hu J, Wu Y, Li T, Ghosh BK (2019) Consensus control of general linear multiagent systems with antagonistic interactions and communication noises. IEEE Trans Autom Control 64(5):2122–2127
15. Cai YL, Zhang HG, Liang YL, Gao ZY (2020) Reduced-order observer-based robust leader-following control of heterogeneous discrete-time multi-agent systems with system uncertainties. Appl Intell 50:1794–1812
16. Maupong TM, Rapisard P (2017) Data-driven control: a behavioral approach. Syst Control Lett 101:37–43
17. Reynolds CW (1987) Flocks, herds, and schools: a distributed behavioral model. Comput Graph 21(4):25–34
18. Couzin ID, Krause J, Franks NR (2005) Effective leadership and decision-making in animal groups on the move. Nature 433:513–516
19. Vicsek T, Zafeiris A (2012) Collective motion. Phys Rep 517:71–140
20. Aldana M, Dossetti V, Huepe C (2007) Phase transitions in systems of self-propelled agents and related network models. Phys Rev Lett 98:095702
21. Liu MY, Lei XK, Yang PP (2014) Progress of theoretical modelling and empirical studies on collective motion. Chin Sci Bull 59:2464–2483
22. Grünbaum D, Viscido S, Parrish JK (2005) Extracting interactive control algorithms from group dynamics of schooling fish. Coop Control 309:103–117
23. Nagy M, Vásárhelyi G, Pettit B, Mariani R, Vicsek T, Biro D (2013) Context-dependent hierarchies in pigeons. Proc Natl Acad Sci 110:13049–13054
24. Conradt L (2012) Models in animal collective decision-making: Information uncertainty and conflicting preferences. Interface Focus 2:226–240
25. Anderson JR (2004) Cognitive psychology and its implications. Worth Publishers, New York
26. Qiu HX, Duan HB (2020) A multi-objective pigeon-inspired optimization approach to UAV distributed flocking among obstacles. Inf Sci 509:515–529
27. Liang HT, Fu YF, Kang FJ, Gao J, Ning Q (2020) A Behavior-driven Coordination Control Framework for Target Hunting by UUV Intelligent Swarm. IEEE Access 8(1):4838–4859
28. Yang PP, Liu MY, Lei XK, Song C (2016) A novel control algorithm for the self-organized fission behavior of flocking system with time delay. Int J Control Autom Syst 14(4):986–997
29. Khaldi B, Harrou F, Cherif F, Sun Y (2020) Improving robots swarm aggregation performance through the Minkowski distance function. 6th international conference on mechatronics and robotics engineering (ICMRE), Barcelona, Spain, pp 87–91
30. Chen C, Chen G, Guo L (2017) On the minimum number of neighbors needed for consensus of flocks. Control Theory Technol 15: 327–339
31. Massé B, Ba S, Horaud R (2018) Tracking gaze and visual focus of attention of people involved in social interaction. IEEE Trans Pattern Anal Mach Intell 40(11):2711–2724
32. Herbert JE, Perna A, Mann RP, Schaerf TM, Sumpter DJT, Ward AJW (2011) Inferring the rules of interaction of shoaling fish. Proc Natl Acad Sci 108:18726–18731
33. Duan H, Huo M, Shi Y (2020) Limit-cycle-based mutant multiobjective pigeon-inspired optimization. IEEE Trans Evol Comput 24(5):948–959
34. Katz Y, Tunstrøm K, Ioannou CC, Huepe C, Couzin ID (2011) Inferring the structure and dynamics of interactions in schooling fish. Proc Natl Acad Sci 108:1870–1872
35. Godsil C, Royle G (2001) Algebraic graph theory. Springer-Verlag, Berlin
36. Yan ZP, Liu YB, Zhou JJ, Zhang W, Wang L (2017) Consensus of multiple autonomous underwater vehicles with double independent Markovian switching topologies and timevarying delays. Chin Phys B 26(4):040203
37. Zhang XY, Jia SM, Li XZ (2017) Improving the synchronization speed of self-propelled particles with restricted vision via randomly changing the line of sight. Nonlinear Dyn 90:43–51
38. Li P, Duan HB (2019) A flocking model based on selective attention mechanics. Sci Sin Technol 49(9):1040–1050
39. Yang PP, Tang Y, Song JC (2018) Self-organized fission/fusion method for flocking system based on predictive intelligence. Control Decis 33(12):2270–2276
40. Dai S, He S, Lin H, Wang C (2018) Platoon formation control with prescribed performance guarantees for USVs. IEEE Trans Ind Electron 65(5):4237–4246

Hongtao Liang received the Ph.D. degree from the Northwestern Polytechnic University (NWPU), Shaanxi, China, in 2017. From 2016 to 2017, he was a Visiting Scholar with the Department of Electrical & Computer Engineering (ECE), National University of Singapore (NUS). He is currently an Assisted professor with School of Physics and Information Technology, Shaanxi Normal University, Shaanxi, China. He has authored or co-authored over 30 papers and holds 18 patents. His research focuses on crowded UUV swarm, cooperative control, pattern recognition, bio-inspired computing and image processing. He was awarded Excellent Doctoral Dissertation Award of China Simulation Society (2018), Outstanding Ph.D. Student Award (2018), and Excellent Doctoral Dissertation Award of Northwestern Polytechnic University (2020).

Yanfang Fu received the Ph.D. degree from Northwestern Polytechnic University (NWPU), Shaanxi, China, in 2008. She is currently a professor with School of Computer Science & Engineering, Xi'an Technological University, Shaanxi, China. Her research focuses on system control and modeling, and Multi-UUV formation control.

Jie Gao received the Ph.D. degree from the Northwestern Polytechnic University (NWPU), Shaanxi, China, in 2013. She is currently an Associate Professor with School of Physics and Information Technology, Shaanxi Normal University, Shaanxi, China. She has authored or co-authored over 20 papers. Her research focuses on unmanned underwater vehicle, and human-computer interaction.